Imaging of HSV-*tk* Reporter Gene Expression: Comparison Between [^{18}F]FEAU, [^{18}F]FFEAU, and Other Imaging Probes

Tadashi Miyagawa[1], George Gogiberidze[1], Inna Serganova[1], Shangde Cai[2], Julius A. Balatoni[1,2], Howard T. Thaler[3], Lyudmila Ageyeva[1], Nagavarakishore Pillarsetty[1,2,4], Ronald D. Finn[2,4,5], and Ronald G. Blasberg[1,4,5]

[1]Department of Neurology, Memorial Sloan-Kettering Cancer Center, New York, New York; [2]Radiochemistry/Cyclotron Core Facility, Memorial Sloan-Kettering Cancer Center, New York, New York; [3]Department of Epidemiology and Biostatistics, Memorial Sloan-Kettering Cancer Center, New York, New York; [4]Department of Radiology, Memorial Sloan-Kettering Cancer Center, New York, New York; and [5]Molecular Pharmacology and Chemistry Program, Memorial Sloan-Kettering Cancer Center, New York, New York

Herpes virus type 1 thymidine kinase (HSV1-*tk*) and the mutant HSV1-*sr39tk* are the 2 most widely used "reporter genes" for radiotracer-based imaging. Two pyrimidine nucleoside analogs, [^{18}F]FEAU (1-(2′-deoxy-2′-fluoro-β-D-arabinofuranosyl)-5-ethyluridine) and [^{18}F]FFEAU (1-(2′-deoxy-2′-fluoro-β-D-arabinofuranosyl)-5-(2-fluoroethyl)uridine), have generated recent interest as potential new probes for imaging HSV1-*tk* and HSV1-*sr39tk* gene expression. **Methods:** We compared [^{18}F]FEAU and [^{18}F]FFEAU with a series of other pyrimidine nucleoside derivatives (including 1-(2′-deoxy-2′-fluoro-β-D-arabinofuranosyl)-5-iodouridine [FIAU]) and with acycloguanosine analogs using a stable HSV1-*tk* transduced cell line (RG2TK+) and wild-type RG2 cells. **Results:** The in vitro accumulation data and the calculated and normalized clearance constant, nKi, as well as sensitivity and selectivity indices indicated that 2 pyrimidine nucleoside probes, [^{18}F]FEAU and [^{18}F]FFEAU, had the best uptake characteristics. These probes were selected for further dynamic PET studies in nude rats bearing subcutaneous RG2TK+ and RG2 tumors. The 2-h postinjection [^{18}F]FEAU uptake levels were 3.3% ± 1.0% and 0.28% ± 0.07% dose/cm^3 in subcutaneous RG2TK+ and RG2 tumors, respectively, and 2.3% ± 0.2% and 0.19% ± 0.01% dose/cm^3, respectively, for [^{18}F]FFEAU. The corresponding RG2TK+/RG2 uptake ratios were 11.5 ± 1.5 and 12.2 ± 1.4, respectively. The inherent problem of comparing different radiolabeled pyrimidine nucleoside and guanosine-based probes for imaging HSV1-*tk* expression using different transduced cell lines and assay systems in the absence of an independent thymidine kinase–enzyme assay is discussed. **Conclusion:** For HSV1-*tk* reporter systems that require a 1- to 4-h PET paradigm, HSV1-*tk*-[^{18}F]FEAU is the current top contender.

Key Words: HSV1-*tk*; herpes simplex virus type 1 thymidine kinase; PET; FEAU; FFEAU; FIAU; ^{18}F; reporter gene

J Nucl Med 2008; 49:637–648
DOI: 10.2967/jnumed.107.046227

The 2 most widely used "reporter genes" for radiotracer-based imaging are herpes virus type 1 thymidine kinase (HSV1-*tk*) and the mutant HSV1-*sr39tk*. The enzyme, wild-type HSV1 thymidine kinase (HSV1-TK), preferentially phosphorylates thymidine and pyrimidine nucleotides derivatives, whereas the mutant enzyme, HSV1-sr39TK, preferentially phosphorylates acycloguanosine derivatives. There have been several publications comparing the uptake and imaging characteristics of different radiolabeled probes for imaging HSV1-*tk* and HSV1-*sr39tk* gene expression, and these publications have presented somewhat inconsistent and confusing results (*1–5*). One of the problems associated with comparing different radiolabeled pyrimidine nucleoside- and guanosine-based probes is that most studies only report a comparison between transduced and wild-type cells or tumors. There is usually no independent measure of HSV1-TK enzyme activity in the transduced cell line or tumor that is used to test efficacy, and this makes it almost impossible to rigorously compare different studies. We know that the level of HSV1-TK enzyme expression is different in different transduced cells and tissue that have been reported in the literature (*6,7*). Furthermore, it has been shown that cell proliferation rate correlates with thymidine kinase transcriptional activation (*8*) and nucleoside transporter function (*9*) as well as thymidine uptake and phosphorylation. Another potential confounding factor is the effect of adenoviral transfection or retroviral transduction on radiolabeled probe uptake in different transduced cells (*3,10*). Thus, HSV1-TK and HSV1-sr39TK probe efficacy comparisons derived from a review of the literature and a comparison of different studies are qualitative at best.

To address this issue, we have performed sequential radiotracer uptake studies comparing different radiolabeled pyrimidine nucleoside probes using a stable HSV1-*tk* transduced cell line and wild-type cell line (RG2TK+ and RG2, respectively) and imaged animals bearing subcutaneous tumors generated from these cell lines. These studies provide

Received Aug. 9, 2007; revision accepted Dec. 4, 2007.
For correspondence or reprints contact: Ronald Blasberg, MD, 1275 York Ave. (Box 52), New York, NY 10021.
E-mail: Blasberg@neuro1.mskcc.org

the best direct in vitro and in vivo comparisons of different radiolabeled probes for imaging HSV1-*tk* expression, in the absence of a direct independent measure of reporter enzyme in the cells or tissue of interest.

There has been recent interest in two ^{18}F-labeled thymidine analogs, [^{18}F]FEAU (1-(2′-deoxy-2′-fluoro-β-D-arabinofuranosyl)-5-ethyluridine) (*11–14*) and [^{18}F]FFEAU (1-(2′-deoxy-2′-fluoro-β-D-arabinofuranosyl)-5-(2-fluoroethyl)uridine) (*15*), as potential new probes for imaging HSV1-*tk* and HSV1-*sr39tk* gene expression. FEAU was first synthesized in the mid-1980s, along with other pyrimidine nucleoside analogs including FIAU (1-(2′-deoxy-2′-fluoro-β-D-arabinofuranosyl)-5-iodouridine), FMAU (1-(2′-deoxy-2′-fluoro-β-D-arabinofuranosyl)-5-methyluridine), FIAC (1-(2′-deoxy-2′-fluoro-β-D-arabinofuranosyl)-5-iodocytosine), and others, as antiviral agents in the treatment of cytomegalovirus *(16)*, herpes simplex virus (*17–19*), and hepatitis virus (*20*) infection. Preliminary results with radiolabeled FEAU and FFEAU have indicated that these compounds have good uptake characteristics in HSV1-*tk* and HSV1-*sr39tk* transduced cells, little or no uptake in nontransduced wild-type cells, and have lower abdominal background activity in mice and rats (*11,14*) compared with that obtained with [^{18}F]FHBG (9-[4-fluoro-3-(hydoxymethyl)butyl]guanine) and [^{124}I]FIAU (1-(2′-deoxy-2′-fluoro-β-D-arabinofuranosyl)-5-iodouridine) (*2*).

For these reasons we compared FEAU and FFEAU with a series of other pyrimidine nucleoside derivatives (including FIAU) and with acycloguanosine analogs using a well-established in vitro uptake assay in the RG2TK+ cell line that has maintained stable levels of HSV1-*tk* expression for over 13 y. We calculate and compare a normalized accumulation (medium clearance) constant (Ki) for each of the radiolabeled probes, and we calculate sensitivity and selectivity indices based on the 50% inhibitory concentration (IC_{50}) of RG2TK+ and RG2 cells to the antiviral drug, ganciclovir (GCV), as an independent measure of HSV1-*tk* expression. We also performed sequential [^{18}F]FEAU and [^{18}F]FFEAU PET studies in the same animals for paired comparisons and for comparison with a previously reported study involving [^{124}I]FIAU, [^{18}F]FHBG, and [^{18}F]FHPG imaging using the same animal model and experimental paradigm (*2*). These results indicate that [^{18}F]FEAU and [^{18}F]FFEAU are better than [^{124}I]FIAU and the ^{18}F-labeled guanosine analogs (FHBG and FHPG) for imaging HSV1-TK 1–2 h after probe administration.

MATERIALS AND METHODS

Cell Lines

The RG2 rat glioma cell line was kindly provided by Darell Bigner (Duke University Medical Center, Durham, NC). RG2 cells were transduced with the recombinant replication-deficient STK retrovirus containing the NeoR gene and HSV1-*tk* gene. The transduced cell line, RG2TK+, has been characterized previously (*1*).

[^{18}F]FEAU and [^{18}F]FFEAU Synthesis

With minor chemical modifications, [^{18}F]FEAU was synthesized by coupling the radiolabeled fluoro-sugar to the silylated pyrimidine derivative following a procedure reported by Alauddin et al. (*21*). The specific activity of the product was ~37 GBq/μmol (~1 Ci/μmol) and the radiochemical purity was >98% after purification by high-performance liquid chromatography (HPLC). The product was formulated in 0.9% NaCl containing 5% ethanol to a total volume based on about 370 MBq/mL (10 mCi/mL) and terminally sterilized by filtration.

The preparation and radiolabeling of FFEAU with ^{18}F was recently described (*15*). Specific activity was estimated to be on the order of 1.5–2.6 GBq/μmol (0.04–0.07 Ci/μmol), on the basis of carrier *n*-Bu_4NF added and the radiochemical yields obtained, and radiochemical purity was 95% as determined by radio–thin-layer chromatography (TLC).

See Supplemental Figure 1 and the supplemental description of the syntheses (supplemental material is available online only at http://jnm.snmjournals.org).

^{14}C- and ^{3}H-Labeled Thymidine and Acycloguanosine Analogs

In vitro uptake studies included the commercially obtained radiolabeled compounds listed in Table 1.

In Vitro Assays

Octanol/Water Partition Coefficients. Octanol/water partition coefficients were determined for [^{18}F]FEAU, [^{18}F]FFEAU, [^{14}C]-FIAU, and [^{3}H]TdR (1-(2′-deoxy)-5-methyluridine) [thymidine]) at 4 pH values of 6.4, 7.0, 7.4, and 8.4 (Table 4), by measuring the distribution of radiolabeled compound in 1-octanol and phosphate-buffered saline (PBS) as described previously (*22*). The log *P* values were calculated using the formula: $\log_{10} P = \log_{10}$ (counts in 1 g of octanol/counts in 1 g of water).

Cell Uptake Studies. RG2TK+ and RG2 cells in culture were used to compare the accumulation of each of the thymidine or acycloguanine analogs with [^{3}H]TdR or [^{14}C]TdR in paired double-label studies (Table 3). Radiotracer accumulation experiments were run over 120 or 180 min and the thymidine- and acycloguanine-analog data were normalized to TdR accumulation as previously described (*1*). In a second set of experiments, the incubation medium contained [^{18}F]FEAU, [^{14}C]FIAU, and [^{3}H]TdR or [^{18}F]FFEAU, [^{14}C]FIAU, and [^{3}H]TdR at the molar medium concentrations shown in Table 1.

The radioactivity assay for the in vitro tissue culture studies involved ^{18}F γ-counting (AutoGamma 5550 spectrometer; Packard Instruments) immediately after the experiment, which was followed 24–36 h later by ^{3}H and ^{14}C β-isotope counting (Tri-Carb Liquid Scintillation Analyzer, model 1600TR; Packard Instruments) using external standard quench correction and standard dual-counting techniques. All data were expressed as disintegrations per minute (dpm)/g cells (or dpm/mL medium). The net accumulation rate (Ki) was calculated from the slope of the probe accumulation versus time plot (dpm/g cells ÷ dpm/mL medium vs. time; units = mL medium/min/g cells—a clearance constant from the incubation medium) and normalized to that of TdR (normalized Ki [nKi]), as the rate of cell proliferation was found to influence the rate of tracer uptake (*1,8,9*).

Sensitivity and Selectivity Indices. To evaluate and compare the proficiency of different probes for imaging HSV1-*tk* expression, 2 indices were developed: sensitivity, defined as the change in probe

TABLE 1
In Vitro Uptake Studies on Commercially Obtained Radiolabeled Compounds

Thymidine analogs	Specific activity (GBg/mmol)	Specific activity (Ci/mmol)	Radiochemical purity (%)	Incubation medium molar concentration (nmol/L)	Company
2′-Fluoro arabinosyl					
[^{18}F]FEAU	~37,000	~1,000	≥98%	~0.4	MSKCC
[^{18}F]FFEAU	15,000–26,000	400–700	≥95%	~0.57–1.0	MSKCC
[^{3}H]TdR	740–1,110	20–30	≥97%	3.3–5.0	Moravek Biochemicals
[^{14}C]TdR	1.85–2.22	0.05–0.06	≥98%	167–200	Moravek Biochemicals
[^{3}H]FEAU	555–1,480	15–40	≥97%	2.5–6.7	Moravek Biochemicals
[^{14}C]FIAU	1.67–2.22	0.045–0.060	≥98%	167–222	Moravek Biochemicals
[^{14}C]FBrAU	1.92	0.054	≥97%	193	Moravek Biochemicals
[^{3}H]FMAU	14.8–111	0.4–3.0	≥97%	33–250	Moravek Biochemicals
[^{3}H]FFAU	370–555	10–15/mmol	≥97%	6.7–10	Moravek Biochemicals
3′-Fluoro ribosyl					
[^{14}C]FLT	2.4	0.065	≥98%	154	Moravek Biochemicals
[^{3}H]FLT	74–370	2–10	≥97%	10–50	Moravek Biochemicals
Ribosyl					
[^{3}H]BrUdR	555–925	15–25	≥97%	4.0–6.7	Moravek Biochemicals
[^{3}H]IUdR	555–740	15–20	≥97%	5.0–6.7	Moravek Biochemicals

MSKCC = Memorial Sloan-Kettering Cancer Center.

uptake (normalized to TdR) divided by the change in HSV1-*tk* expression independently measured by GCV IC_{50}, and selectivity, defined as "sensitivity" divided by substrate uptake due to endogenous (mammalian) TK. These 2 related measures were considered useful for establishing in vitro assay criteria that would likely reflect in vivo imaging considerations—namely, maximum image signal intensity (e.g., high sensitivity) and maximum image contrast (the ability to differentiate between HSV1-TK and endogenous TK—e.g., high selectivity). Neither of these indices represents a fraction of some ideal value (i.e., they do not have an absolute or maximum value). Rather, they provide indices for a direct comparison of different probes and are normalized to the expression level of HSV1-*tk* (GCV IC_{50}) and endogenous mammalian TK in the cell systems used for the comparisons. The sensitivity and selectivity indices were calculated from:

$$\text{Probe Sensitivity} = \Delta(\text{Probe}/\text{TdR})/\Delta(\text{GCV IC}_{50}).$$

$$\text{Probe Selectivity} = \text{Sensitivity}/(\text{probe}/\text{TdR}) \text{ for RG2 cells.}$$

Subcutaneous Tumors and Animal Imaging Studies

The experimental protocol involving animals was approved by the Institutional Animal Care and Use Committee of the Memorial Sloan-Kettering Cancer Center. Subcutaneous tumors were produced in *rnu/rnu* rats (200–250 g; Frederick Cancer Center) by subcutaneous injection of 5×10^6 tumor cells in 200 μL of serum-free cell culture medium under anesthesia (ketamine [87 mg/kg] and kylazine [13 mg/kg], intraperitoneal). Transduced RG2TK+ cells were placed in the left shoulder (test) and wild-type RG2 cells were placed in the right shoulder (negative control). The animals were monitored for tumor growth by daily measurements of the tumor size and the animal weight. Animals were studied when the subcutaneous tumors reached a diameter of ~15 mm, 7–14 d after subcutaneous implantation of the RG2 and RG2TK+ cells. The growth rate, macroscopic and microscopic appearances, as well as the degree of vascularization were similar in both the HSV1-*tk* transduced and the wild-type subcutaneous tumors.

PET

Sequential studies with [^{18}F]FEAU and [^{18}F]FFEAU were performed on the same animals on consecutive days. All animals were anesthetized with ketamine (87 mg/kg) and xylazine (13 mg/kg) administered intraperitoneally. Five animals were first injected with [^{18}F]FEAU (2.22–4.81 MBq/animal [60–130 μCi/animal] intravenous) and imaged over 2 h; on the following day they were injected with [^{18}F]FFEAU (629–925 kBq/ animal [17–25 μCi/animal] intravenous) and reimaged over 2 h. Only 3 animals were imaged with [^{18}F]FFEAU because of low radiopharmaceutical yield (*13*).

PET was performed using the Advance Tomograph (GE Healthcare) (see supplemental imaging tomograph characteristics, settings, and paradigm). Regional tumor radioactivity concentrations (%ID/cm^3), decay-corrected to time of injection, were estimated from the maximum pixel within regions of interest drawn around the tumor on transaxial slices of the reconstructed image sets, and radioactivity was plotted at the acquisition midpoint.

Statistical Analysis

Statistical significance of comparisons between [^{18}F]FEAU, [^{18}F]FFEAU, and [^{14}C]FIAU was based on an ANCOVA to compare the slopes of linear fits of the data versus [^{3}H]TdR (Fig. 2). Two-sided paired Student *t* tests were used for TdR nKi, sensitivity, and selectivity values (Table 3) in RG2TK+ and RG2 cells, and the in RG2TK+/RG2 ratio values (Supplemental Table 2). Logarithmic transformations were used when appropriate to bring the data into closer agreement with implicit assumptions of normal statistical distributions with constant variance.

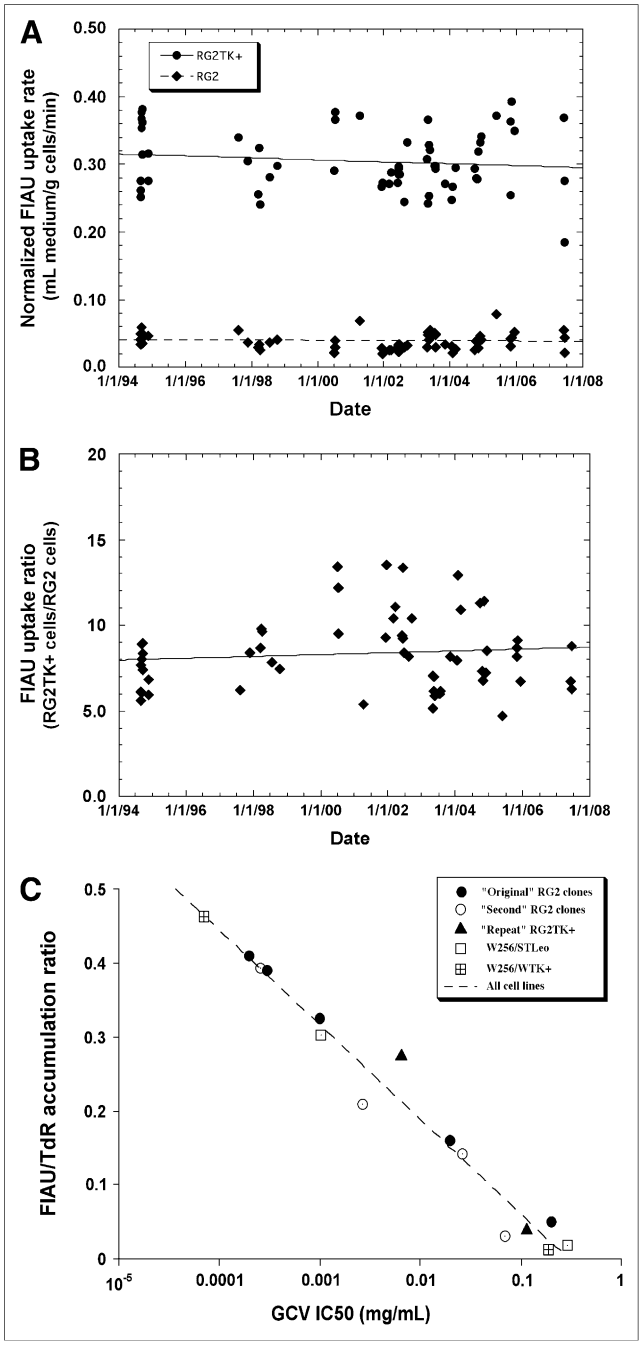

FIGURE 1. Paired nucleoside ([^{14}C]FIAU and [^{3}H]TdR) accumulation studies in RG2TK+ transduced cells and wild-type RG2 cells are shown over the course of a 13-y period (August 1994–June 2007). Accumulation rate (mL medium/min/g cells; Ki) of [^{14}C]FIAU for transduced RG2TK+ cells (solid circles) and RG2 wild-type cells (solid diamonds) is normalized to that of [^{3}H]TdR (A) (*1*). Each point represents the slope of paired [^{14}C]FIAU and [^{3}H]TdR uptake experiments conducted between 10 and 180 min or 30 and 120 min. A linear fit of the plots yielded a slope of -4.4 ± 4.9 ($\times 10^{-11}$) and -0.91 ± 1.3 ($\times 10^{-11}$) Ki units/d for RG2TK+ and RG2 cells, respectively, which was not significantly different from zero. The ratio of Ki values in paired RG2TK+ and RG2 experiments over the same time period was plotted (B); the slope of the plot is 1.7 ± 2.3 ($\times 10^{-9}$) d^{-1} and also was not significantly different from zero. The relationship of the FIAU/TdR uptake ratio and GCV EC_{50} values for different TK-expressing clones is shown (C); the initial (1994) values obtained for RG2TK+ and RG2 cells are shown (solid circles); the current (2007) values are shown (solid triangles).

RESULTS

RG2TK+ Cell Line Stability

The level of HSV1-TK expression in RG2TK+ and RG2 cells, as measured by the TdR-normalized uptake (clearance) rate constant for FIAU, has remained stable over 13 y (Fig. 1A); the slopes of the linear fits through the data points in Figure 1A are not significantly different from zero. Similarly, the RG2TK+/RG2 uptake ratio was constant over the 13 y, and the slope of a linear fit through the data points was not significantly different from zero (Fig. 1B). An independent measure of the level and stability of HSV1-*tk* expression in RG2TK+ cells is provided by sensitivity measures (IC_{50}) to the antiviral drug GCV. Recently determined IC_{50} values for GCV were 6.5 ± 0.7 and 116 ± 15 μg/mL for RG2TK+ and RG2 cells, respectively (Fig. 1C, solid diamond); they were found to remain stable and compare favorably with the IC_{50} values initially reported for these cell lines (*1*).

In Vitro Assays

The lipophilicity (octanol/water partition coefficient) of [^{3}H]FEAU and [^{18}F]FFEAU were determined and compared with that of [^{14}C]FIAU and [^{3}H]TdR over a range of pH values (Table 2). The log *P* values of [^{18}F]FEAU, [^{18}F]FFEAU, and [^{3}H]TdR were stable between pH 6.4 and 8.4, whereas the lipophilicity of [^{14}C]FIAU decreased above pH 7.4.

A comparison of different radiolabeled compounds as potential probes for imaging HSV1-*tk* gene expression are listed on the basis of their structural characteristics (Table 3). The accumulation rate constants (nKi) in RG2TK+ and RG2 cells, normalized to that of thymidine (*1*), were highest for the 2′-fluor-arabinosyl and ribosyl analogs in RG2TK+ cells. The acyclo-guanosine analogs tend to have the lowest Ki values in RG2TK+ cells. In wild-type (non–HSV1-*tk* expressing) RG2 cells, the Ki value reflects mammalian thymidine kinase (TK1 plus TK2) activity. Not surprisingly, the ribosyl and 3′-ribosyl analogs had the highest nKi values in RG2 cells, and the acyclo-guanosine analogs had very low nKi values in RG2 cells. Sensitivity and selectivity indices were calculated from the uptake data and the GCV IC_{50} values for the transduced RG2TK+ and wild-type RG2 cell lines (*1*) (Table 3). The rank-order of compounds displayed within each subset of Table 3 is based on the sensitivity index. The differences between the values obtained with [^{18}F]FEAU and [^{18}F]FFEAU were significant for nKi in RG2TK+ cells ($P < 0.0001$; *t* test, unequal variance) and in RG2 cells ($P < 0.05$) and for the sensitivity index ($P < 0.001$), but there was no difference in the selectivity index between the 2 probes (Table 3). The difference in the RG2TK+/RG2 ratio (Supplemental Table 2) was also highly significant ($P < 0.0001$).

TABLE 2
log *P* Values at Different pH Values

Compound	pH 6.4	pH 7.0	pH 7.4	pH 8.4
[^{18}F]FEAU	−0.076 ± −0.002	−0.062 ± −0.001	−0.082 ± −0.002	−0.086 ± −0.001
[^{18}F]FFEAU	−0.35 ± 0.02	−0.32 ± 0.01	−0.30 ± 0.01	−0.29 ± −0.03
[^{14}C]FIAU	−0.055 ± −0.002	−0.074 ± −0.005	−0.096 ± −0.001	−0.42 ± 0.02
[^{3}H]TdR	−0.99 ± 0.07	−1.00 ± −0.07	−1.00 ± −0.02	−1.00 ± −0.02

Values are mean; ± SD (n = 2).

A more rigorous comparison of [^{18}F]FEAU and [^{14}C]FIAU accumulation normalized to that of [^{3}H]TdR was performed in a series of 8 triple-label experiments (Fig. 2A). The uptake of [^{18}F]FEAU and [^{14}C]FIAU uptake in both transduced (RG2TK+) and wild-type (RG2) cells was less than that of TdR. The slopes of the [^{18}F]FEAU and [^{14}C]FIAU plots were significantly different ($P < 0.001$) in RG2TK+ cells, and the nKi values calculated from the slopes were 0.70 ± 0.05 (SEE) and 0.31 ± 0.01 mL/min/g for FEAU and FIAU, respectively. The reverse relationship was observed in RG2 cells, where there was very little uptake of FEAU in the wild-type cells. The nKi values in RG2 cells were also significantly different ($P < 0.0001$); 0.049 ± 0.002 and 0.0018 ± 0.0009 mL/min/g for FIAU

TABLE 3
RG2TK+ and RG2 Cellular Uptake Studies

Analog	nKi: RG2TK+ (mL/min/g)	nKi: RG2 (mL/min/g)	Sensitivity* (× 10^3)	Selectivity†	No. of experiments‡
Thymidine§					
2′-Fluoro arabinosyl					
[^{18}F]FEAU	0.84 ± 0. 22	0.0014 ± 0.0004	4.2 ± 1.1	3.3 ± 1.7	7
[^{18}F]FFEAU‖	0.27 ± 0.03	0.00064 ± 0.00055	1.4 ± 0.2	2.8 ± 2.7	6
[^{14}C]FIAU	0.30 ± 0.05	0.040 ± 0.012	1.3 ± 0.2	0.037 ± 0.011	66
[^{3}H]FBrAU	0.29 ± 0.07	0.12 ± 0.04	0.86 ± 0.38	0.0089 ± 0.0065	10
[^{3}H]FMAU	0.21 ± 0.03	0.065 ± 0.010	0.71 ± 0.16	0.011 ± 0.004	3
[^{18}F]FTMAU¶	0.051 ± 0.006	0.0028 ± 0.0020	0.24 ± 0.03	0.052 ± 0.016	3
[^{18}F]FBrVAU¶	0.029 ± 0.004	−0.0080 ± 0.0163	0.18 ± 0.07	−0,44 ± 0.82	4
[^{3}H]FFAU	0.042 ± 0.006	0.011 ± 0.003	0.16 ± 0.02	0.015 ± 0.003	3
[^{18}F]FPAU#	0.014 ± 0.003	−0.0007 ± 0.0008	0.074 ± 0.012	−0.13 ± 0.33	3
2′-Fluoro ribosyl					
[^{3}H]FIRU	0.070 ± 0.018	0.0011 ± 0.0005	0.35 ± 0.09	0.39 ± 0.22	6
[^{3}H]FMRU	0.019 ± 0.006	0.00081 ± 0.00008	0.093 ± 0.029	0.11 ± 0.02	3
3′-Fluoro ribosyl					
[^{14}C]FLT	0.064 ± 0.025	0.12 ± 0.04	−0.26 ± 0.06	−0.0023 ± 0.0003	6
Ribosyl					
[^{3}H]BrUdR	0.54 ± 0.07	0.47 ± 0.05	0.44 ± 0.21	0.0010 ± 0.0005	4
[^{3}H]IUdR	0.38 ± 0.01	0.32 ± 0.01	0.32 ± 0.04	0.0010 ± 0.0001	3
Acyclo guanosine					
[^{18}F]FHBG**	0.023 ± 0.002	0.0033 ± 0.0013	0.10 ± 0.02	0.035 ± 0.019	2
[^{3}H]GCV††	0.015 ± 0.005	0.0023 ± 0.0002	0.062 ± 0.026	0.027 ± 0.009	3
[^{18}F]FHPG**	0.0078 ± 0.0004	0.00042 ± 0.00019	0.037 ± 0.001	0.099 ± 0.043	2
[^{3}H]ACV††	0.0068 ± 0.0013	0.0039 ± 0.0013	0.015 ± 0.001	0.0040 ± 0.0012	3

*Sensitivity = Δ (Probe/TdR)/Δ (GCV IC_{50}).
†Selectivity = Sensitivity‡/(probe/TdR) for RG2 cells.
‡Number of concurrent RG2TK+ and RG2 experiments.
§Ranked according to magnitude of sensitivity value in each analog group.
‖Includes 3 separate experiments previously reported by Balatoni et al. (*15*).
¶From (*28*).
#From (*22*).
**From (*2*).
††From (*1*).
Values are the mean ± SD.

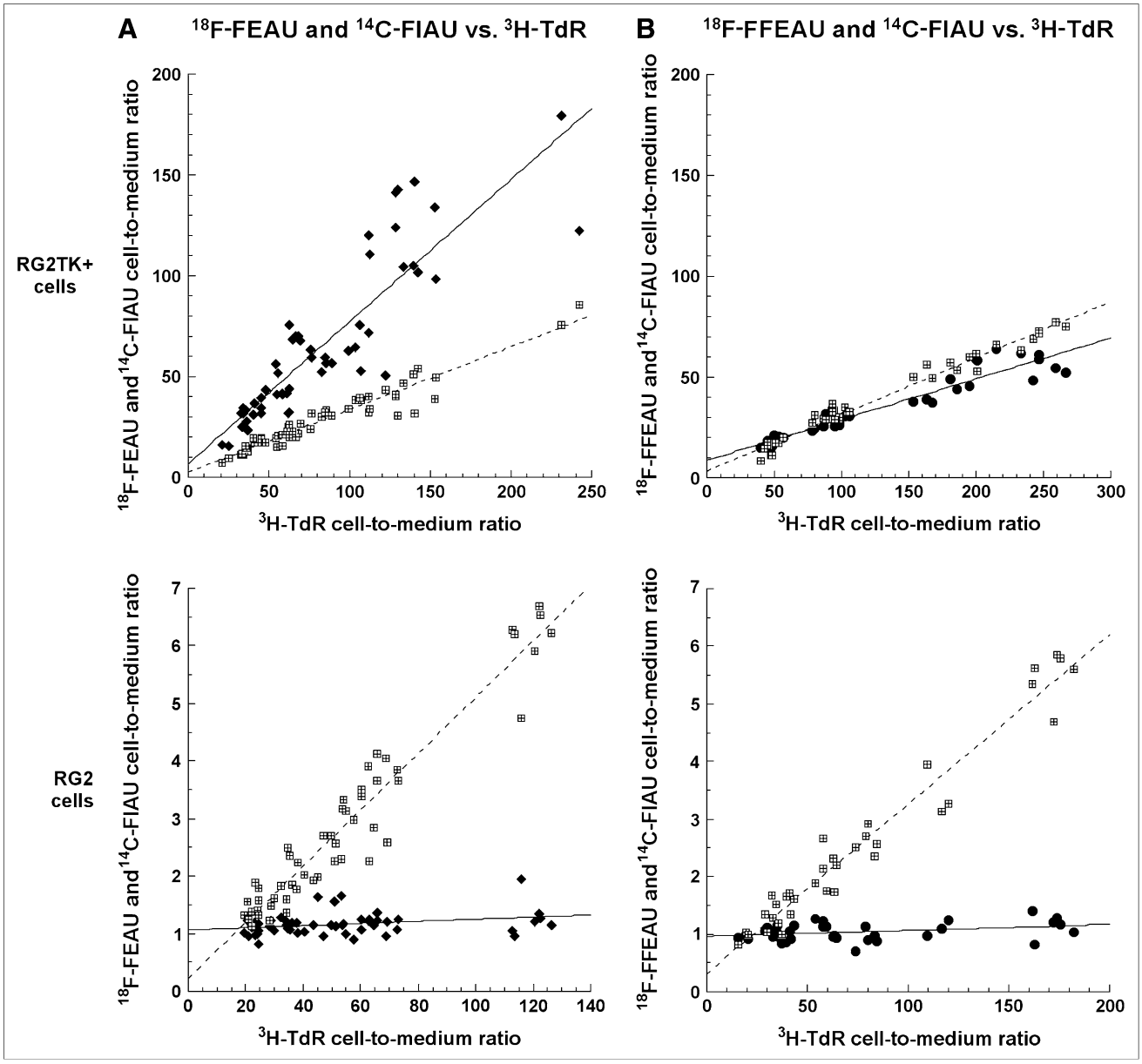

FIGURE 2. Paired, triple-label nucleoside accumulation studies in RG2TK+ transduced cells and wild-type RG2 cells are shown for [^{18}F]FEAU (A, left column) and [^{18}F]FFEAU (B, right column) in a comparison with [^{14}C]FIAU and [^{3}H]TdR. The accumulation (mL medium/g cells) of [^{18}F]FEAU (solid diamonds) and [^{18}F]FFEAU (solid circles) are compared with that of [^{14}C]FIAU (hatched squares) and normalized to corresponding [^{3}H]TdR values (abscissa) (*1*). Results obtained in RG2TK+ cells are shown in upper panels and those obtained in RG2 cells are shown in lower panels.

and FEAU, respectively. These results are similar to those calculated in Table 3.

A similar triple-label study comparing the accumulation of [^{18}F]FFEAU and [^{14}C]FIAU with that of [^{3}H]TdR in RG2TK+ and RG2 cells was also performed (Fig. 2B). The slope of the [^{18}F]FFEAU plot was slightly less ($P < 0.001$) than that for [^{14}C]FIAU in RG2TK+ cells; the nKi values calculated from the slopes were 0.20 ± 0.01 and 0.28 ± 0.01 mL/min/g for FFEAU and FIAU, respectively. In RG2 cells there was very little uptake of FFEAU compared with that of FIAU; the nKi values were significantly different ($P < 0.0001$); 0.0010 ± 0.0004 and 0.030 ± 0.001 mL/min/g for FFEAU and FIAU, respectively). These results are similar to that previously reported (*15*). Comparing the slopes of [^{18}F]FEAU (Fig. 2A) and [^{18}F]FFEAU (Fig. 2B) shows them to be significantly different ($P < 0.0001$) in RG2TK+ cells but not in RG2 cells.

A graphical comparison of the nKi values for ^{18}F probes obtained in paired RG2TK+ and RG2 cell uptake studies shows that the probes cluster roughly into 4 groups (Fig. 3A). The upper-left quadrant is the optimal location for potential HSV1-TK imaging probes in this plot, with high nKi values

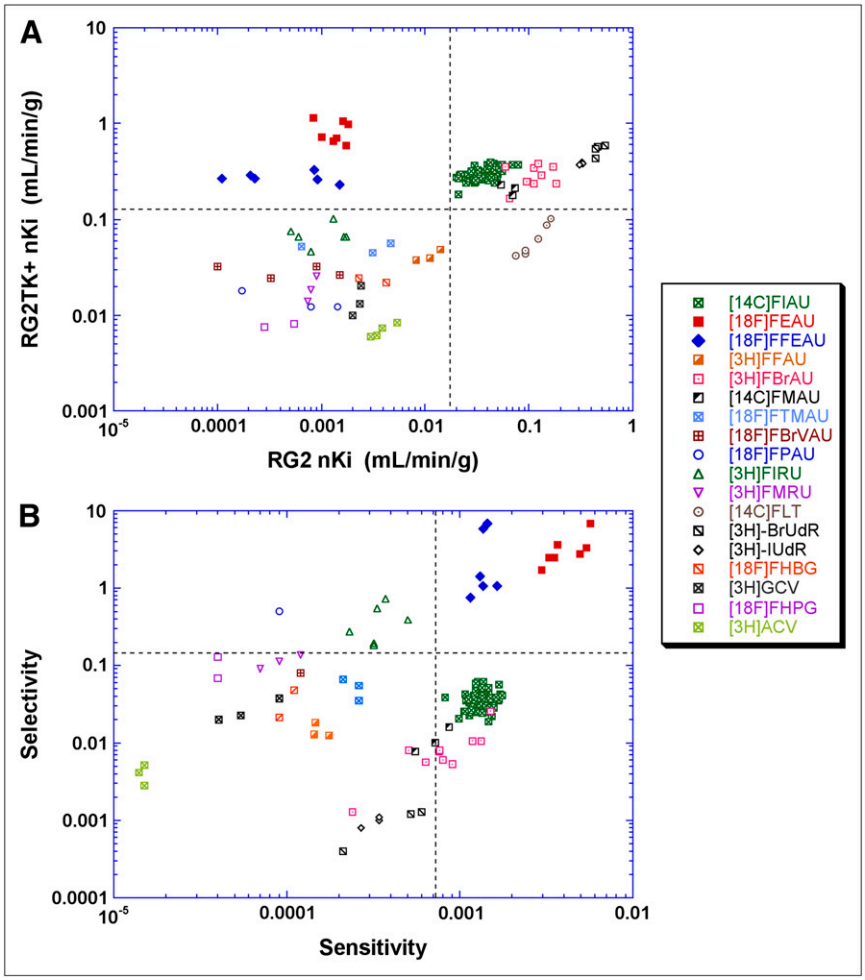

FIGURE 3. Probe comparisons based on nKi values obtained in paired RG2TK+ and RG2 cell uptake studies (A) and comparison of calculated sensitivity–selectivity indices (B). Each point represents an individual experiment.

in RG2TK+ cells and low nKi values in RG2 cells. This quadrant includes FEAU and FFEAU. The upper-right quadrant includes probes with relatively high nKi values in both RG2TK+ and RG2 cells; FIAU is the best probe in this group, which also contains FMAU, FBrAU (1-(2′-deoxy-2′-fluoro-β-D-arabinofuranosyl)-5-bromouridine), IUdR (1-(2′-deoxy)-5-iodoouridine), and BrUdR (1-(2′-deoxy)-5-bromouridine). The lower-left quadrant includes 10 probes with relatively low nKi values in both RG2TK+ and RG2 cells; FIRU (1-(2′-deoxy-2′-fluoro-β-D-ribofuranosyl)-5-iodouridine) and FTMAU (1-(2′-deoxy-2′-fluoro-β-D-arabinofuranosyl)-5-fluorouridine) are the best probes in this group, which also contains FFAU (1-(2′-deoxy-2′-fluoro-β-D-arabinofuranosyl)-5-fluorouridine), FBrVAU (1-(2′-deoxy-2′-fluoro-β-D-arabinofuranosyl)-5-(2-bromovinyl) uridine), FMRU (1-(2′-deoxy-2′-fluoro-β-D-ribofuranosyl)-5-methyluridine), FHBG, FPAU (1-(2′-deoxy-2′-fluoro-β-D-arabinofuranosyl)-5-propyluridine), GCV (9-[(2-hydroxy-1-(hydroxymethyl)ethoxy)methyl]guanine), FHPG (9-[(3-fluoro-1-hydoxy-2-propoxy)methyl]guanine), and ACV (9-[(2-hydroxy-1-ethoxy)methyl]guanine [acyclovir]). The lower-right quadrant represents the worst location in the plot, with relatively low nKi values in RG2TK+ cells and high nKi values in RG2 cells; only FLT (3′-deoxy-3′-fluorothymidine) falls in this quadrant. A similar comparison plot of probe sensitivity and selectivity indices is shown in Figure 3B. The optimal quadrant (upper-right, high sensitivity and high selectivity) contains FEAU and FFEAU; the least-optimal quadrant (lower-left, low sensitivity and low selectivity) is less clearly defined and includes several of the probes. The least ideal probes shown in Figure 3B include ACV, BrUdR, and IUdR; FLT must also be included in this group but was not plotted because of negative sensitivity and selectivity indices.

In Vivo Imaging

The in vitro results presented suggest that both [^{18}F]FEAU and [^{18}F]FFEAU would be good probes for imaging HSV1-*tk* expression in animals. A comparison of sequential [^{18}F]FEAU and [^{18}F]FFEAU Advance (GE Healthcare) PET images of the same *rnu/rnu* rat is shown in Figure 4. The sequence of 10-min imaging frames demonstrates rapid accumulation of radioactivity in the RG2TK+ tumor, with no visualization of the wild-type RG2 tumor above background levels. Although total-body background activity is relatively high in the initial 10-min frame, it drops fairly rapidly. The sequential images show that renal clearance is

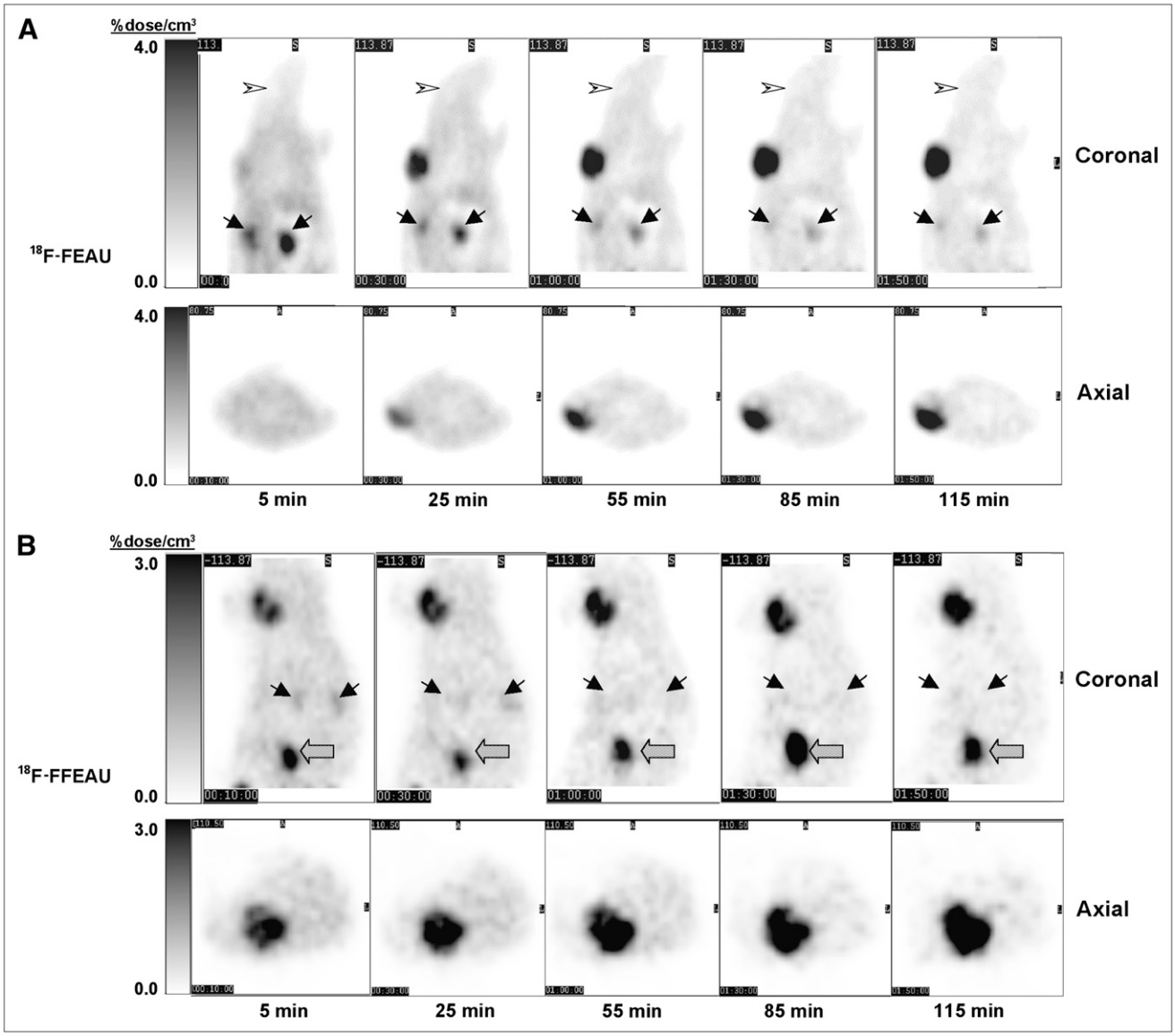

FIGURE 4. Comparison of [^{18}F]FEAU images (upper 2 panels) and [^{18}F]FFEAU images (lower 2 panels) of the same *rnu/rnu* rat, bearing 2 subcutaneous tumors: RG2TK+ tumor on right shoulder and wild-type RG2 tumor on left shoulder. Imaging was performed on sequential days; serial 10-min imaging frames were obtained after intravenous injection of radiopharmaceutical. Single coronal and axial slices through RG2TK+ and RG2 tumors are presented, and image time is the midpoint of a 10-min acquisition. Image intensity scale is the same for all frames. The brain is indicated by a stylized arrow in A; the brain was above field of view in B. Kidneys are indicated by a solid arrow; urinary bladder is indicated by the open arrow in B but was below the field of view in A.

the predominant route of excretion for both [^{18}F]FEAU and [^{18}F]FFEAU. The kidneys were clearly visible during the early postinjection images and then became less distinct; the urinary bladder radioactivity increased during the 2-h imaging period for both radiopharmaceuticals. There was little or no accumulation of either radiopharmaceutical in most organ systems outside of the urinary tract, including liver and intestine. No ex vivo, postimaging tissue radioactivity assays were performed in this study because of the sequential imaging of [^{18}F]FEAU and [^{18}F]FFEAU in the same cohort of animals.

The radioactivity accumulation profiles of [^{18}F]FEAU and [^{18}F]FFEAU in RG2TK+ and RG2 tumors in the same set of animals were obtained from the sequential images that are shown in Figure 5. Also included are the corresponding accumulation profiles of [^{124}I]FIAU; the FIAU profiles are presented for reference and were generated from data previously published (*2*), using the same animal model and PET tomograph. Both [^{18}F]FEAU and [^{18}F]FFEAU accumulate rapidly in RG2TK+ tumors over the first 45 min and then tend to plateau. The level of [^{18}F]FEAU radioactivity in RG2TK+ tumors at 45 and 115 min was 2.1% ± 0.4% and 3.3% ± 1.0% dose/cm^3, respectively; the corresponding values for [^{18}F]FFEAU were 1.8% ± 0.3% and 2.3% ± 0.2% dose/cm^3, respectively. In contrast, [^{124}I]FIAU accumulates very rapidly and plateaus early in RG2TK+ tumors (*2*).

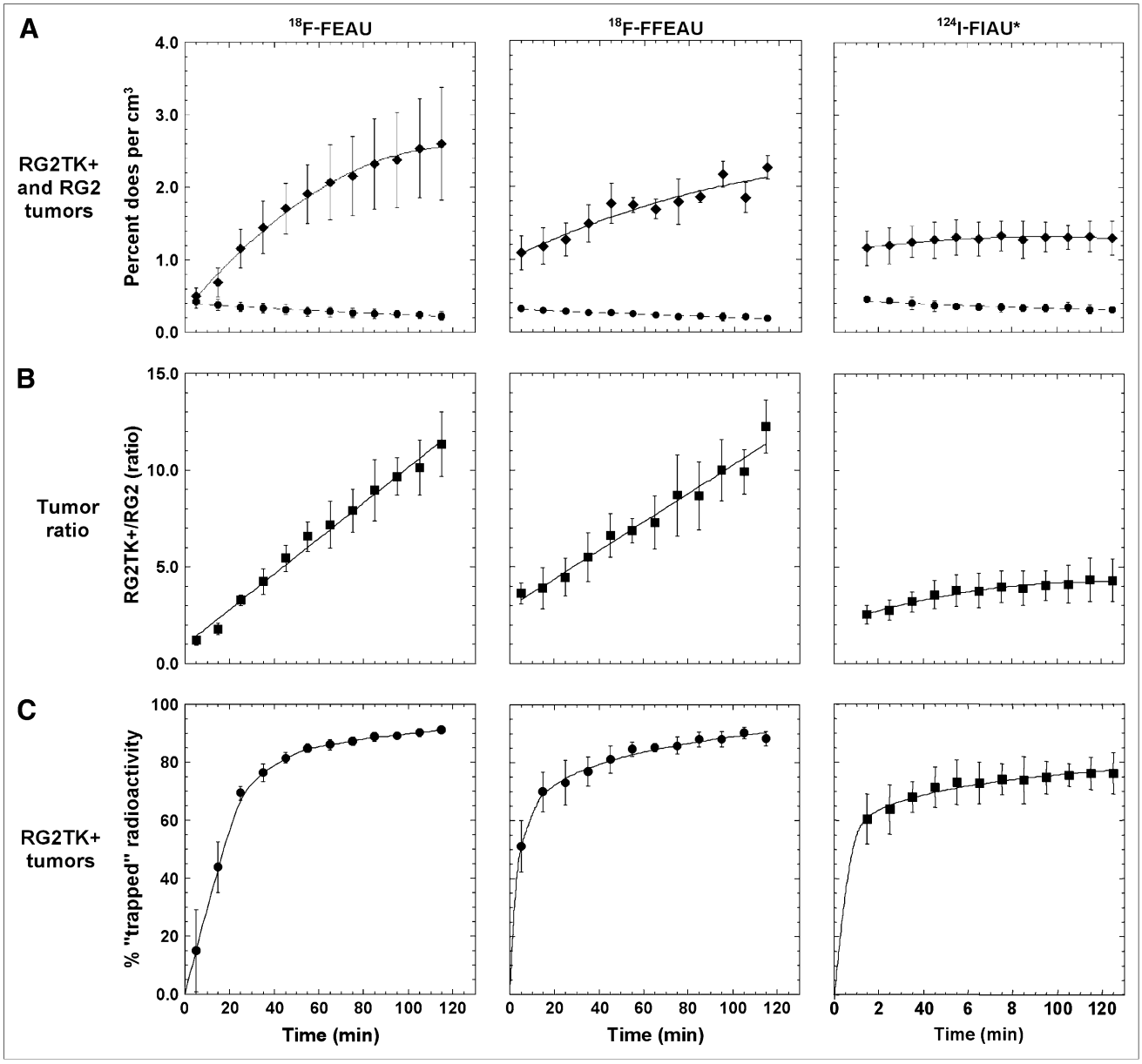

FIGURE 5. Radioactivity–time profiles of [^{18}F]FEAU, [^{18}F]FFEAU, and [^{124}I]FIAU* in RG2TK+ and RG2 tumors. *rnu/rnu* rats bearing 2 subcutaneous tumors, RG2TK+ tumor on right shoulder and wild-type RG2 tumor on left shoulder, were imaged. Serial 10-min imaging frames were obtained after intravenous injection of radiopharmaceutical. Maximum voxel values (% dose/cm^3) measured in each tumor (RG2TK+, solid diamond; RD2, solid circle), at mid point of each 10-min acquisition, are plotted (A). Corresponding (RG2TK+)/(RG2) radioactivity ratio is also plotted (B). Percent radioactivity above background levels (% "trapped") was calculated: % "trapped" radioactivity = 100[(RG2TK+) − (RG2)]/(RD2TK+) (C). Values are mean, ± SD. FEAU (n = 5) and FFEAU (n = 3) data were obtained from same set of animals imaged on consecutive days (the available FFEAU radiopharmaceutical was sufficient for only 3 animals); FIAU* data profile (*2*) is provided for reference.

[^{124}I]FIAU radioactivity levels at 45 and 125 min were 1.27% ± 0.25% and 1.30% ± 0.23% dose/cm^3, respectively (*2*). In contrast, the corresponding 2-h values in wild-type RG2 tumors were low: 0.28% ± 0.07%, 0.19% ± 0.01%, and 0.31% ± 0.05% dose/cm^3 for the 3 probes, respectively.

Radioactivity clearance from wild-type RG2 tumors was exponential for all 3 nucleosides. The clearance half-time ($t_{1/2}$) of [^{18}F]FEAU from RG2 tumors was 126 ± 7 min (SEE); for [^{18}F]FFEAU, the clearance half-time was 149 ± 9 min (Supplemental Table 1). FIAU clearance from RG2 tumors was exponential but was slightly slower ($t_{1/2}$ = 211 ± 3 min) than that of FEAU and FFEAU.

The transduced tumor–to–wild-type tumor activity ratio was time-dependent and increased linearly for both FEAU and FFEAU over the 120-min imaging period (Fig. 5B). The percent radioactivity above background levels (% "trapped") in RG2TK+ tumors increased rapidly but required approximately 50 min to reach 80% of the total

measured value for both FEAU and FFEAU and >120 min for FIAU (Fig. 5C).

The uptake and clearance profiles of [^{18}F]FEAU- and [^{18}F]FFEAU-derived radioactivity in various organ structures were obtained from the dynamic PET data (Supplemental Fig. 2). The half-times for [^{18}F]FEAU and [^{18}F]FFEAU clearance were similar (~2 h) in most organs, except for more rapid renal clearance, ($t_{1/2}$ = ~55 min). Bladder radioactivity increased from ~2% to ~20% dose/cm^3 over the 120-min experimental period for both FEAU and FFEAU. See Supplemental Table 1 clearance data.

DISCUSSION

The objective of this study was to compare several different radiolabeled thymidine and acycloguanosine analogs as potentially better probes for imaging HSV1-*tk* expression. The RG2 rat glioma and transduced RG2TK+ cell lines were chosen for these experiments, as our initial studies were performed with these cell lines (*1*), and HSV1-*tk* expression in the RG2TK+ cell line has remained stable since that time (Fig. 1). These cell lines provide a consistent in vitro assay system for measuring and comparing HSV1-*tk* dependent accumulation of the different probes using a standard cell-culture radiotracer uptake assay (*1*).

The in vitro accumulation data and the calculated sensitivity and selectivity values (Table 3 and Fig. 3) indicated that 2 pyrimidine nucleoside probes, [^{18}F]FEAU and [^{18}F]FFEAU, had the best uptake characteristics and they were selected for further dynamic imaging studies in an established tumor animal model. These imaging results are also comparable with previously reported findings (*2*), as the same animal model bearing RG2TK+ and RG2 tumors and the same PET scanner were used in generating the image data.

[^{18}F]FEAU and [^{18}F]FFEAU yielded similar imaging results and similar tissue uptake and clearance profiles. High RG2TK+/RG2 radioactivity ratios, >10:1, were imaged by 90 min with both probes. The ratios for FEAU and FFEAU at 2 h were similar (12.2 ± 1.4 and 11.3 ± 1.7, respectively) and were ~3-fold higher than comparable measurements obtained with FIAU at 2 h (4.3 ± 1.1; $P < 0.0001$), and they are markedly higher than that measured with FHBG (2.3 ± 0.6; $P < 0.0001$) and FHPG (1.2 ± 0.3; $P < 0.0001$) ((*2*) and listed in Supplemental Table 2). It is important to note that the RG2TK+/RG2 ratios were linearly increasing over the 120-min period of imaging, indicating that the ratio is a time-dependent value. It should also be noted that the RG2TK+/RG2 radioactivity ratio for [^{124}I]FIAU at 24 h was considerably higher, 65 ± 21 (*2*), and demonstrates the advantage of a late-imaging paradigm due to the retention of [^{124}I]FIAU in HSV1-*tk*–expressing tissue and the greater clearance of [^{124}I]FIAU from the body at 24 h compared with 2 h (*2,23*).

Background thoracic and abdominal activity was comparatively low; radioactivity clearance half-times from most organs were approximately 2 h. The route of body clearance was predominantly renal; the highest levels of radioactivity in the body were observed in kidney and bladder. Notably, only low levels of radioactivity were found in liver and intestine, and the stomach was not identifiable on the images. This is in sharp contrast to the much higher levels that were observed in liver and intestine with [^{18}F]FHPG and [^{18}F]FHBG and in stomach with [^{124}I]FIAU (*2*). In contrast, we and others have observed high intestinal (background) activity after [^{18}F]FEAU administration in mice (*11,14*). The reason for this difference in the level of [^{18}F]FEAU intestinal (background) activity in mice compared with that in rats is currently being investigated. Others, however, have not observed high [^{18}F]FEAU intestinal uptake in mice (*13*).

The octanol/water partition coefficient of FEAU is similar to that of FIAU and is slightly higher than that of FFEAU and TdR. The log *P* values indicate low lipid solubility and suggest that these substrates will not cross cerebral capillaries rapidly. This is consistent with the low levels of FEAU and FFEAU radioactivity visualized in the brain of these animals (Fig. 4A). Thus, FEAU and FFEAU are not likely to be useful probes for imaging HSV1-*tk* expression behind an intact blood–brain barrier.

The radiochemistry, both in synthesis time and yield, was different for the 2 pyrimidine nucleosides. [^{18}F]FFEAU was synthesized using a straightforward, 2-step procedure involving fluorination of the tresyl precursor, which was followed by deprotection of the benzoyl groups and final purification of the compound using HPLC. The time of synthesis was about 90–120 min when conducted manually (automation of the steps would shorten synthesis time). However, radiochemical yields averaged ~0.2% (decay-corrected), with radiochemical purity ranging from 91% to 98% (*15*). In contrast, the synthesis of [^{18}F]FEAU is a multistep procedure (*21*). The total time of synthesis for [^{18}F]FEAU was approximately 180–220 min, with radiochemical yields of 10%–30% (decay-corrected), and radiochemical purity was >98%. Although the imaging characteristics of HSV1-*tk* expression and biodistribution of [^{18}F]FFEAU are similar to that of [^{18}F]FEAU, the superior radiochemical yields of [^{18}F]FEAU—in spite of the long, complicated multistep synthesis—clearly favor FEAU over FFEAU. It was our expectation that the simpler direct radiosynthesis of [^{18}F]FFEAU would lead to an imaging agent that can be readily adapted to automated synthetic modules for radiofluorination.

Since 2002, when we reported our comparisons between [^{124}I]FIAU, [^{18}F]FHBG, and [^{18}F]FHPG for imaging HSV1-*tk* expression in rats bearing RG2 and RG2TK+ tumors (*2*), there have been several studies comparing the uptake of different radiolabeled probes. They include comparisons between radiolabeled pyrimidine nucleosides (FIAU. FEAU, FMAU, FBrAU, and FFAU) (*3,4,10–13,15,21–29*) as well as acycloguanosine nucleosides (FHBG, FHPG, and PCV) (*3,4,10,21,24*) using different transduced cell lines expressing either HSV1-*tk* and HSV1-*tksr39*. The sequential in vivo imaging studies reported here demonstrated that FEAU and

FFEAU accumulation (% injected dose/cm^3) was high in RG2TK+ tumors and low in RG2 tumors and in different organs (Figs. 3 and 4). For a tracer with a 110-min half-life, the clearance of radioactivity from nontransduced tissues was rapid, and excretion was predominantly renal and consistent with log *P* values ranging from −0.08 (FEAU) to −0.3 (FFEAU) at pH 7.4 (Table 2). Our in vivo results were also compared with other recent studies that assessed the uptake of different pyrimidine and acycloguanosine radiotracers in different HSV1-*tk* and HSV1-*tksr39* transduced tumors (see the supplemental comparison of HSV1-*tk* and HSV1-*tksr39* imaging probes). In this comparison, FEAU shows consistent high levels of accumulation in transduced cells and tumors, with little or no accumulation in wild-type cells and tumors. The picture is less consistent in a comparison of the animal models. This may reflect differences in the host animal (*rnu/rnu* rat vs. athymic nude mouse), radionuclide and site of labeling (e.g., [^{18}F]FEAU vs. [^{3}H]FEAU), or other factors (e.g., image region-of-interest measures vs. tissue sampling and well counting).

It should also be noted that [^{124}I]FIAU has one distinct advantage over the ^{18}F-labeled substrates; the 4-d half-life of this radionuclide provides the opportunity for late, high-contrast imaging when background activity is low. The RG2TK+/RG2 tumor radioactivity ratio obtained from tissue sampling ex vivo measurements increased from 9–11 at 2 h to 65 at 24 h (*2*). It should also be noted that the RG2TK+/RG2 tumor radioactivity ratio increased linearly with time over the 2-h imaging session, indicating that any presentation of results as a target-to-background ratio must consider the time-dependent characteristic of such a ratio (Fig. 5B) and that imaging at least 50 min after FEAU or FFEAU injection is required to ensure at least 80% of measured radioactivity represents trapped, non-background radioactivity (Fig. 5C).

Although these results highlight the advantages of [^{124}I]FIAU and late imaging involving a constitutively expressed HSV1-*tk* reporter system, concern has been raised about the ability of HSV1-*tk* reporter systems to image transcriptional gene regulation involving inducible promoters that require multiple, sequential imaging studies. The issue of HSV1-TK enzyme stability in living cells was investigated recently and compared with that of firefly luciferase (*30*). Dynamic gene expression studies in transduced sarcoma cells showed that the luciferase gene was a better reporter gene for monitoring short, dynamic transcriptional events (enzyme $t_{1/2}$ ~2–3 h (*31,32*)), whereas HSV1-TK protein was shown to have a half-life of about 35 h (*30*). Although the long half-life of HSV1-TK reporter protein may be a problem for monitoring rapidly changing biologic processes with inducible promoters coupled to HSV1-*tk*, this issue is much less important in the use of constitutive promoters coupled to HSV1-*tk* reporters in cell-tracking studies.

We previously discussed a major problem in comparing different radiolabeled pyrimidine nucleoside and guanosine-based probes (*2*). Namely, there is no reference to the amount of HSV1-*tk* gene product or enzyme present in the transduced cells or tumors. Most studies report only a comparison between transduced and wild-type cells or tumors and present no independent measure of HSV1-TK enzyme activity in the transduced cell line or tumor that is used to test efficacy. Because the level of HSV1-TK enzyme expression is likely to vary in different transduced cells and tissues reported in the literature, it is not possible to rigorously compare the results reported in many of these studies.

We have addressed this issue differently by comparing different probes in single transduced and wild-type cell lines, RG2TK+ and RG2, which have maintained a stable level of HSV1-*tk* expression over 13 y (Figs. 1A and 1B) and have maintained similar levels of sensitivity (IC_{50}) to an antiviral drug, GCV (Fig. 1C). Thus, the comparisons between different radiolabeled thymidine and acycloguanosine analogs reported here (Table 3 and Supplemental Table 2) are considered to be reliable comparisons, even though they were performed over different periods of time. In addition, multilabeling of [^{18}F]FEAU and [^{18}F]FFEAU were performed along with [^{14}C]FIAU and [^{3}H]TdR, which provided direct paired comparisons (Fig. 2), and the same cohort of tumor-bearing animals was imaged with [^{18}F]FEAU and [^{18}F]FFEAU on consecutive days.

CONCLUSION

[^{18}F]FEAU will have an important role to play in HSV1-*tk* reporter gene imaging in the future. On the basis of radiosynthetic yield, our in vitro and in vivo results and those of others, [^{18}F]FEAU is currently the best ^{18}F-radiopharmaceutical for imaging HSV1-*tk* expression. It remains to be determined if this is also the case for HSV1-*tksr39*.

ACKNOWLEDGMENTS

This work was supported by NIH grants P50 CA86438 and R24 CA83084 and by DOE grant FG03-86ER60407. We thank Bradley Beattie for his support in providing access to and maintenance of the image files and Revathi Desai for expert technical assistance with the early in vitro radiotracer uptake studies (MSKCC).

REFERENCES

1. Tjuvajev JG, Stockhammer G, Desai R, et al. Imaging the expression of transfected genes *in vivo*. *Cancer Res.* 1995;55:6126–6132.
2. Tjuvajev J, Doubrovin M, Akhurst T, et al. Comparison of radiolabeled nucleoside probes (FIAU, FHBG, and FHPG) for PET imaging of HSV1-*tk* gene expression. *J Nucl Med.* 2002;43:1072–1083.
3. Min JJ, Iyer M, Gambhir SS. Comparison of [^{18}F]FHBG and [^{14}C]FIAU for imaging of HSV1-*tk* reporter gene expression: adenoviral infection vs stable transfection. *Eur J Nucl Med Mol Imaging.* 2003;30:1547–1560.
4. Kang KW, Min JJ, Chen X, Gambhir SS. Comparison of [^{14}C]FMAU, [^{3}H]FEAU, [^{14}C]FIAU, and [^{3}H]PCV for monitoring reporter gene expression of wild type and mutant herpes simplex virus type 1 thymidine kinase in cell culture. *Mol Imaging Biol.* 2005;7:296–303.
5. Serganova I, Ponomarev V, Blasberg RG. Human reporter genes: potential use in clinical studies. *Nucl Med Biol.* 2007;34:791–807.

6. Ponomarev V, Doubrovin M, Serganova I, et al. A novel triple-modality reporter gene for whole-body fluorescent, bioluminescent, and nuclear noninvasive imaging. *Eur J Nucl Med Mol Imaging.* 2004;31:740–751.
7. Ray P, Tsien R, Gambhir SS. Construction and validation of improved triple fusion reporter gene vectors for molecular imaging of living subjects. *Cancer Res.* 2007;67:3085–3093.
8. Dou QP, Pardee AB. Transcriptional activation of thymidine kinase, a marker for cell cycle control. *Prog Nucleic Acid Res Mol Biol.* 1996;53:197–217.
9. Pastor-Anglada M, Casado FJ, Valdés R, Mata J, García-Manteiga J, Molina M. Complex regulation of nucleoside transporter expression in epithelial and immune system cells. *Mol Membr Biol.* 2001;18:81–85.
10. Alauddin MM, Shahinian A, Gordon EM, Conti PS. Direct comparison of radiolabeled probes FMAU, FHBG, and FHPG as PET imaging agents for HSV1-*tk* expression in a human breast cancer model. *Mol Imaging.* 2004;3:76–84.
11. Serganova I, Doubrovin M, Vider J, et al. Molecular imaging of temporal dynamics and spatial heterogeneity of hypoxia-inducible factor-1 signal transduction activity in tumors in living mice. *Cancer Res.* 2004;64:6101–6108.
12. Buursma AR, Rutgers V, Hospers GA, Mulder NH, Vaalburg W, de Vries EF. ^{18}F-FEAU as a radiotracer for herpes simplex virus thymidine kinase gene expression: in-vitro comparison with other PET tracers. *Nucl Med Commun.* 2006;27:25–30.
13. Alauddin MM, Shahinian A, Park R, Tohme M, Fissekis JD, Conti PS. *In vivo* evaluation of 2′-deoxy-2′-[^{18}F]fluoro-5-iodo-1-beta-D-arabinofuranosyluracil ([^{18}F]FIAU) and 2′-deoxy-2′-[^{18}F]fluoro-5-ethyl-1-beta-D-arabinofuranosyluracil ([^{18}F]FEAU) as markers for suicide gene expression. *Eur J Nucl Med Mol Imaging.* 2007;34:822–829.
14. Tseng JC, Zanzonico PB, Levin B, Finn R, Larson SM, Meruelo D. Tumor-specific in vivo transfection with HSV-1 thymidine kinase gene using a Sindbis viral vector as a basis for prodrug ganciclovir activation and PET. *J Nucl Med.* 2006;47:1136–1143.
15. Balatoni JA, Doubrovin M, Ageyeva L, et al. Imaging herpes viral thymidine kinase-1 reporter gene expression with a new ^{18}F-labeled probe: 2′-fluoro-2′-deoxy-5-[^{18}F]fluoroethyl-1-beta-d-arabinofuranosyl uracil. *Nucl Med Biol.* 2005;32:811–819.
16. Colacino JM, Lopez C. Efficacy and selectivity of some nucleoside analogs as anti-human cytomegalovirus agents. *Antimicrob Agents Chemother.* 1983;24:505–508.
17. Mansuri MM, Ghazzouli I, Chen MS, et al. 1-(2-Deoxy-2-fluoro-beta-D-arabinofuranosyl)-5-ethyluracil: a highly selective antiherpes simplex agent. *J Med Chem.* 1987;30:867–871.
18. Chou TC, Kong XB, Fanucchi MP, et al. Synthesis and biological effects of 2′-fluoro-5-ethyl-1-beta-D-arabinofuranosyluracil. *Antimicrob Agents Chemother.* 1987;31:1355–1358.
19. Kong XB, Scheck AC, Price RW, et al. Incorporation and metabolism of 2′-fluoro-5-substituted arabinosyl pyrimidines and their selective inhibition of viral DNA synthesis in herpes simplex virus type 1 (HSV-1)-infected and mock-infected Vero cells. *Antiviral Res.* 1988;10:153–166.
20. Kong XB, Vidal P, Tong WP, Chiang J, Gloff CA, Chou TC. Preclinical pharmacology and pharmacokinetics of the anti-hepatitis virus agent 2′-fluoro-5-ethyl-1-beta-D-arabinofuranosyluracil in mice and rats. *Antimicrob Agents Chemother.* 1992;36:1472–1477.
21. Alauddin MM, Shahinian A, Gordon EM, Bading JR, Conti PS. Preclinical evaluation of the penciclovir analog 9-(4-[^{18}F]fluoro-3-hydroxymethylbutyl)guanine for in vivo measurement of suicide gene expression with PET. *J Nucl Med.* 2001; 42:1682–1690.
22. Pillarsetty N, Cai S, Ageyeva L, Finn RD, Blasberg RG. Synthesis and evaluation of [^{18}F] labeled pyrimidine nucleosides for positron emission tomography imaging of herpes simplex virus 1 thymidine kinase gene expression. *J Med Chem.* 2006; 49:5377–5381.
23. Tjuvajev JG, Avril N, Oku T, et al. Imaging herpes virus thymidine kinase gene transfer and expression by positron emission tomography. *Cancer Res.* 1998;58: 4333–4341.
24. Nanda D, de Jong M, Vogels R, et al. Comparison of [^{18}F]FHPG and [$^{124/125}$I]FIAU for imaging herpes simplex virus type 1 thymidine kinase gene expression. *Eur J Nucl Med.* 2001;28:721–729.
25. Alauddin MM, Shahinian A, Park R, Tohme M, Fissekis JD, Conti PS. Synthesis and evaluation of 2′-deoxy-2′-^{18}F-fluoro-5-fluoro-1-beta-D-arabinofuranosyluracil as a potential PET imaging agent for suicide gene expression. *J Nucl Med.* 2004;45:2063–2069.
26. Alauddin MM, Shahinian A, Park R, Tohme M, Fissekis JD, Conti PS. Synthesis of 2′-deoxy-2′-[^{18}F]fluoro-5-bromo-1-beta-D-arabinofuranosyluracil ([^{18}F]-FBAU) and 2′-deoxy-2′-[^{18}F]fluoro-5-chloro-1-beta-D-arabinofuranosyl-uracil ([^{18}F]-FCAU), and their biological evaluation as markers for gene expression. *Nucl Med Biol.* 2004;31:399–405.
27. Choi TH, Ahn SH, Kwon HC, Choi CW, Awh OD, Lim SM. *In vivo* comparison of IVDU and IVFRU in HSV1-TK gene expressing tumor bearing rats. *Appl Radiat Isot.* 2004;60:15–21.
28. Cho SY, Ravasi L, Szajek LP, et al. Evaluation of ^{76}Br-FBAU as a PET reporter probe for HSV1-*tk* gene expression imaging using mouse models of human glioma. *J Nucl Med.* 2005;46:1923–1930.
29. Wang HE, Yu HM, Liu RS, et al. Molecular imaging with ^{123}I-FIAU, ^{18}F-FUdR, ^{18}F-FET, and ^{18}F-FDG for monitoring herpes simplex virus type 1 thymidine kinase and ganciclovir prodrug activation gene therapy of cancer. *J Nucl Med.* 2006;47:1161–1171.
30. Hsieh CH, Liu RS, Wang HE, et al. *In vitro* evaluation of herpes simplex virus type 1 thymidine kinase reporter system in dynamic studies of transcriptional gene regulation. *Nucl Med Biol.* 2006;33:653–660.
31. Thompson F, Hayes LS, Lloyd DB. Modulation of firefly luciferase stability and impact on studies of gene regulation. *Gene.* 1991;103:171–177.
32. Ignowski JM, Schaffer DV. Kinetic analysis and modeling of firefly luciferase as a quantitative reporter gene in live mammalian cells. *Biotechnol Bioeng.* 2004;86: 827–834.

JNM The Journal of NUCLEAR MEDICINE

Imaging of HSV-*tk* Reporter Gene Expression: Comparison Between [^{18}F]FEAU, [^{18}F]FFEAU, and Other Imaging Probes

Tadashi Miyagawa, George Gogiberidze, Inna Serganova, Shangde Cai, Julius A. Balatoni, Howard T. Thaler, Lyudmila Ageyeva, Nagavarakishore Pillarsetty, Ronald D. Finn and Ronald G. Blasberg

J Nucl Med. 2008;49:637-648.
Published online: March 14, 2008.
Doi: 10.2967/jnumed.107.046227

The Journal of Nuclear Medicine is published monthly.
SNMMI | Society of Nuclear Medicine and Molecular Imaging
1850 Samuel Morse Drive, Reston, VA 20190.
(Print ISSN: 0161-5505, Online ISSN: 2159-662X)

SNMMI SOCIETY OF NUCLEAR MEDICINE AND MOLECULAR IMAGING